Evolutionary Kinetics of Graphene Formation on Copper

Kemal Celebi,[†] Matthew T. Cole,[‡,||] Jong Won Choi,[†] Frederic Wyczisk,[§] Pierre Legagneux,[§] Nalin Rupesinghe,[||] John Robertson,[‡] Kenneth B. K. Teo,[||] and Hyung Gyu Park*,[†]

[†]Institute of Energy Technology, ETH Zürich, Zürich CH-8092, Switzerland

[‡]Department of Engineering, Electrical Engineering Division, University of Cambridge, Cambridge CB3 0FA, United Kingdom

[§]Thales Research and Technology, Palaiseau Cedex 91767, France

[||]AIXTRON Ltd., Cambridge CB24 4FQ, United Kingdom

S *Supporting Information*

ABSTRACT: It has been claimed that graphene growth on copper by chemical vapor deposition is dominated by crystallization from the surface initially supersaturated with carbon adatoms, which implies that the growth is independent of hydrocarbon addition after the nucleation phase. Here, we present an alternative growth model based on our observations that oppose this claim. Our Gompertzian sigmoidal growth

kinetics and secondary nucleation behavior support the postulate that the growth can be controlled by adsorption−desorption dynamics and the dispersive kinetic processes of catalytic dissociation and dehydrogenation of carbon precursors on copper.

KEYWORDS: Graphene, chemical vapor deposition, Gompertzian sigmoidal growth kinetics, secondary nucleation, dispersive kinetics, catalytic dissociation and dehydrogenation
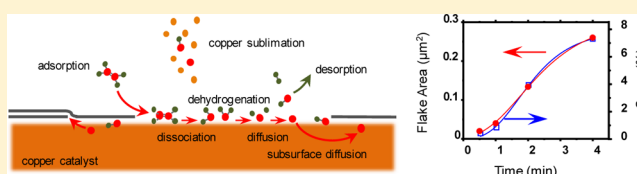
Graphene growth on copper by chemical vapor deposition (CVD) has become the favored approach for synthesizing high quality transferable graphene, due to the potential for large area, increasingly inexpensive, commercially viable production.[1,2] However, utilization of such *en masse* graphene in many applications requires systematic optimization of the CVD processes for obtaining selective single or bilayer growth, as well as highly crystalline, large area domains with high degrees of lattice interconnectivity.[3−5] While in-depth reports on graphene growth kinetics on metals with high carbon affinity, such as Ru and Ir,[6−8] have been reported, studies of the growth kinetics on copper are relatively sparse.[9,10]

Studies on copper-catalyzed graphene CVD have thus far suggested that surface catalysis with associated adsorption, diffusion, dissociation, dehydrogenation, and lattice-attachment steps determines the growth kinetics.[11,12] As hydrocarbons facilitate carbon adsorption on copper surfaces, and the energy barrier for diffusion is low (<1 eV),[13] so far the discussion on the growth mechanism has been primarily focused on the type of the carbon reactant.[14−16] The reactant and reaction type have been a subject of intense debate. Even though there have been theoretical[13] and experimental[17] claims on the complete dehydrogenation of various feedstock hydrocarbons during, or after lattice attachment, some reports base their explanations on carbon adatoms being the single dominant reactant on the copper surface.[9,14]

While the reactant type has been widely discussed, an active discussion on the growth kinetics remains incomplete. It is only very recently that an Avrami model[18] of crystallization from a pool of supersaturated carbon adatoms on the copper surface has been proposed.[9] However, this model was still based on

growth mechanisms on surfaces with significant carbon solubility, applicable for nickel yet questionable for copper. Furthermore, the implicit assumptions of this model were that: (a) carbon adatoms are the sole building block forming the graphene lattice; and (b) no additional carbon input takes place upon initial supersaturation. As mentioned previously, the first assumption has both supporting[14] and conflicting reports,[13,15] whereas the second assumption has not been discussed in any great detail, even though it is unphysical for the hydrocarbon input to suddenly cease adsorption completely on the copper surface as soon as the graphene growth starts.

Here, for the first time, we present data on graphene growth kinetics rationalized via a Gompertz sigmoidal function.[19] Gompertzian kinetics have been observed in single-walled carbon nanotube growth[20] and other organic crystallization processes, such as those associated with fats and oils.[21−24] Our observations support the postulate of continual carbon input onto the copper surface and the crucial role of copper sublimation in determining the growth kinetics and flake morphology. We analyze the associated time-dependent activation energy and suggest that the dispersive kinetics of the catalytic dissociation and dehydrogenation reactions of ethylene to be one possible rate-determining mechanism for graphene growth on copper.
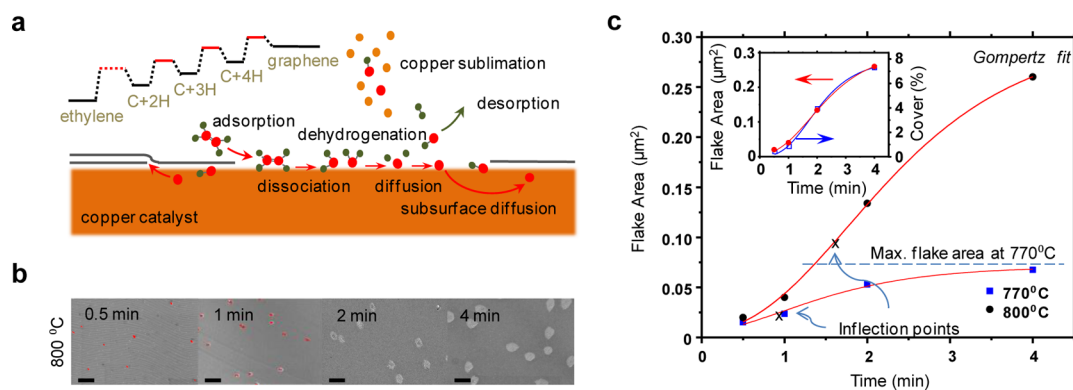
To elucidate the underlying CVD growth kinetics and associated mechanisms (Figure 1a), the evolving flake

Figure 1. CVD growth of graphene on copper. (a) Growth scheme and associated stepwise mechanisms. (b) Representative scanning electron micrographs showing typical flake evolution with time, at 800 °C (scale bar: 1 μm). (c) Evolution of the mean flake area with time. Red curves indicate Gompertz fittings to the flake size data. Inset: Comparison of the measured mean flake size and measured percentage of the graphene area over the entire substrate surface.

morphology was monitored over a parametric window that allows the flakes to be suitably sparse for individual analysis. Focusing on the initial evolution, a growth time window of 0.5−4 min and temperature window of 770−860 °C (with an interval of 30 °C) were selected. A common annealing step was used throughout (900 °C, 30 min, hydrogen (20 sccm): argon (1500 sccm)), followed by ethylene (C$_2$H$_4$) exposure. To ensure negligible chamber contamination, growths under similar conditions in the absence of any carbon precursor were performed. No graphene flakes grew confirming negligible leakage or residual carbon contamination. In situ mass spectroscopy confirmed ethylene as the primary carbon precursor impinging on the copper. Further details on the growth can be found in the Supporting Information (in the methods section and Figure S1).

Figure 1b shows representative scanning electron microscope (SEM) images of some graphene flakes. An example of a complete set of SEM micrographs showing flake evolution is given in the Supporting Information, Figure S2. A clear areal enlargement is visible with increased growth time. The kinetics of this enlargement is illustrated in Figure 1c, which shows the graphene flake area as a function of growth time. The variation in flake area (0.02−0.26 μm^2) compares well with the measured total areal ratio of graphene (Figure 1c, inset). We rationalize our observations by a modified Gompertz function of the form:[25]

$$A(t) = A_{\max} \exp\left\{-\exp\left[-\frac{\mu_{\mathrm{m}} e}{A_{\max}}(t - \lambda) + 1\right]\right\} \quad (1)$$

where A is the graphene flake area (μm^2), $A_{\max}$ is the maximum flake area (μm^2) at the growth saturation, μ_{m} is the maximum growth rate (dA/dt at the inflection point), e is Euler's number, λ is the time lag (min) measured by the abscissa intersection of the tangent drawn from the inflection point, and t is the growth time (min). The recursive least-squares (R^2) was >0.97 throughout. The present model is independent of the copper surface crystallographic orientation. The copper surface consists of extremely large (mm-size) grains, which are (100) orientated and are close to parallel to the surface plane after the growth. The copper grain orientation is independent of the growth temperature and time, as evidenced by electron backscatter diffractometry (Figure S3). Grain orientation maps show few grain boundaries but pervasive lattice bending by 10° or more throughout the grains.

To explain the observed sigmoidal kinetic behavior, we first investigated if the growth duration is determined by the actual duration of hydrocarbon exposure or the total duration at the growth temperature upon hydrocarbon exposure. When the total growth time was kept constant (2 min) and the hydrocarbon flow time was reduced (2 min flow vs 1 min flow plus 1 min no-flow), the flake size decreased, indicating that the growth is in fact sustained by continual hydrocarbon input to the copper surface. However, when the hydrocarbon supply time was kept constant (1 min) and the total duration at the growth temperature was extended (1 min vs 2 min, starting at the onset of the hydrocarbon flow), the flake size did not change, suggesting that the contribution of the initial supersaturated state to the growth is minimal, compared to the continual adsorption after the first nucleation phase.

Second, we consider hydrogen mediated carbon etching. If such an effect can be ruled out, then the growth can be explained simply via carbon reactant kinetics at the copper surface. Pregrown samples were exposed to hydrogen partial pressures and temperatures equivalent to the growth conditions used: typically, hydrogen (20 sccm) at 900 °C. No observable etching of the pregrown graphene was seen. Furthermore, growths without hydrogen showed no measurable difference in flake size from those grown with hydrogen. Thus, we believe that the hydrogen flow rate was suitably low to obviate graphene etching. Indeed, ethylene-based graphitic carbon growth has been shown to be robust against changes in hydrogen partial pressure compared to other carbon feed-stock.[13] Graphene etching was only notable when a significant amount (>300 sccm) of hydrogen was supplied at 1 mbar partial pressure, far away from our process window and extremely uncharacteristic for standard growth conditions.

Three main observations are critical to understand the underlying growth kinetics. First, the observed sigmoidal kinetics has an initially increasing growth rate, which again hints that a continual hydrocarbon feed is the dominant source for carbon reactants on the copper surface. If the initial supersaturation were the dominant carbon source, then the growth rate would monotonically decrease. Thus, we conclude that the effect of the initial carbon reactant supersaturation could possibly only be critical during the nucleation phase. Second, secondary graphene nucleations take place some minutes (ca. 2−4 min) after the first nucleation, and the resultant secondary layers (Figure 2a) cease growth after the
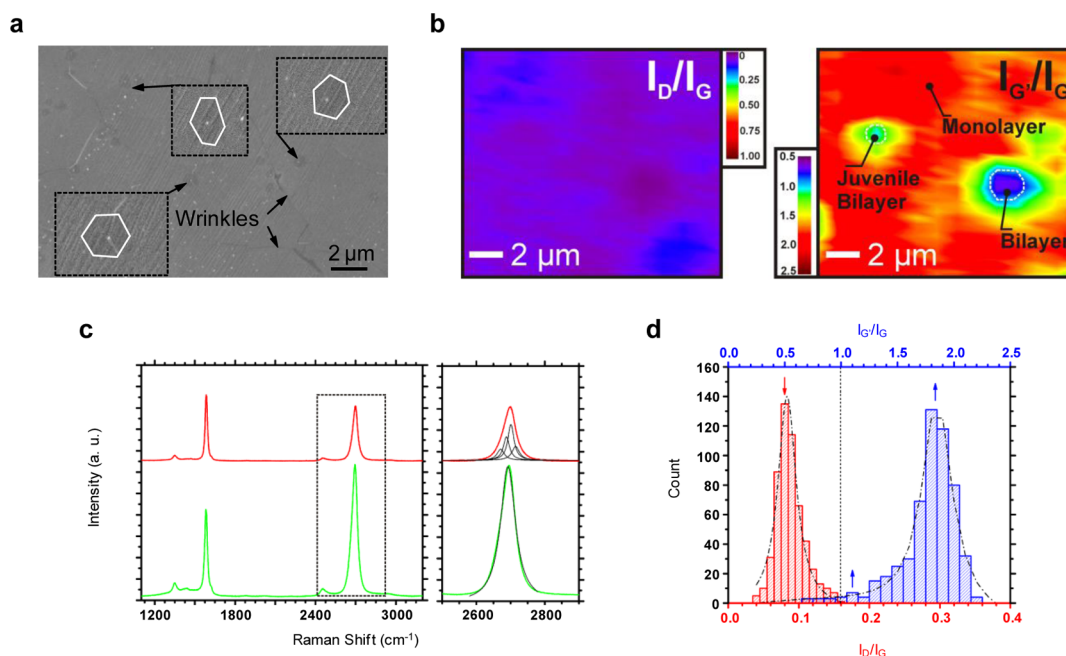
Figure 2. (a) An SEM micrograph of a continuous graphene monolayer. Small secondary layers are magnified to illustrate the hexagonal flake morphology. White lines are drawn at the secondary layer boundaries for visual guidance (scale bar: 2 μm). (b) Raman map of the I_D/I_G and $I_{G'}/I_G$ showing monolayer (red), juvenile bilayer (green), and bilayer (blue) regions (scale bar: 2 μm). (c) Typical 532 nm Raman spectra of a monolayer (green) and bilayer (red) regions with single and 4-fold Lorentzian fits to the G' peak (~2700 cm^{-1}). (d) I_D/I_G (0.09 ± 0.02) and $I_{G'}/I_G$ (1.82 ± 0.25) distributions.

first graphene layer achieves full covering. This observation also supports the continual hydrocarbon input hypothesis and indicates that these secondary graphene flakes possibly exist under the first graphene layer. The carbon reactants can diffuse beneath the first layer, as supported by previous studies.[13,26] Lastly, the secondary graphene flakes adopt hexagonal morphologies due to suppressed copper sublimation under the first graphene layer,[27] while the first layer flakes are rather circular in shape (quantified later in the text). Thus, copper sublimation is an important factor during low-pressure CVD growth of graphene on copper.

Based on the above observations we now present a time-dependent picture of the CVD process (Figure 1a). First, ethylene is adsorbed on the copper. Previous studies suggested that ethylene can polymerize to butadiene at 700−750 °C in the presence of copper but decomposes at higher temperatures.[28] Catalytic decomposition and dehydrogenation are expected in our entire temperature range. As a result, a mixture of carbon adatoms, dimers, and intermediate hydrocarbon species having single or double carbon atoms could form a mixed state of reactants on the copper surface, which can themselves undergo dissociation and dehydrogenation reactions until lattice attachment or desorption occurs. Desorption of these reactants is enhanced on the exposed copper surface via the advancing copper step edges due to copper sublimation. The reactants are free to diffuse with a low energy barrier (<1 eV) on around the surface and subsurface of the copper depending on their detailed constituents.[15,16,29] Carbon reactants can also diffuse beneath the graphene flakes,[26] in which case the enlarging graphene could isolate the surface reactants captured underneath it from sublimation enhanced desorption. Thus, the total amount of surface reactants can increase, while the flakes continue to enlarge after the depletion of the initial carbon supersaturation.

Using the reasoning above we now construct a consistent mathematical model of the growth kinetics. The increase in the available carbon reactant density, due to the inhibited desorption/sublimation beneath the flakes, is presumably proportional to the prolongation of the diffusion time prior to desorption, which is in turn proportional to A. Not all of the carbon reactants may readily attach to the graphene lattice unless they are energetically active and sterically favorable. Cascades of catalytic dissociation and dehydrogenation reactions can lead to the production of the active carbon species that can readily attach to the graphene lattice.[30] This catalytic process may be much slower than the attachment reaction to the graphene lattice (as explained later in the text); thus, reactant attachment to the graphene edge does not limit the growth kinetics (as there is no $(A)^{1/2}$ factor present in our growth model). The characteristic time scales for the variations in reactant density and surface morphology are comparable to the time scales for dissociative dehydrogenation.[27] Hence, the rate constant for the overall reaction is time-dependent, which can be best explained by dispersive kinetics.[31−33] Taking an exponentially decaying formalism for dispersive kinetics, it is possible to write the graphene areal enlargement rate as,

$$\frac{dA}{dt} \propto K(t)n_R \propto A\exp(-kt) \tag{2}$$

where K is the rate of the reaction that produces the active species that can attach to the graphene, n_R is the carbon reactant density, and k represents the exponential coefficient of the time-dependent reaction rate. This proportionality is equivalent to the Gompertzian differential equation, which states

$$\frac{dA}{dt} \propto A\ln(1/A) \tag{3}$$
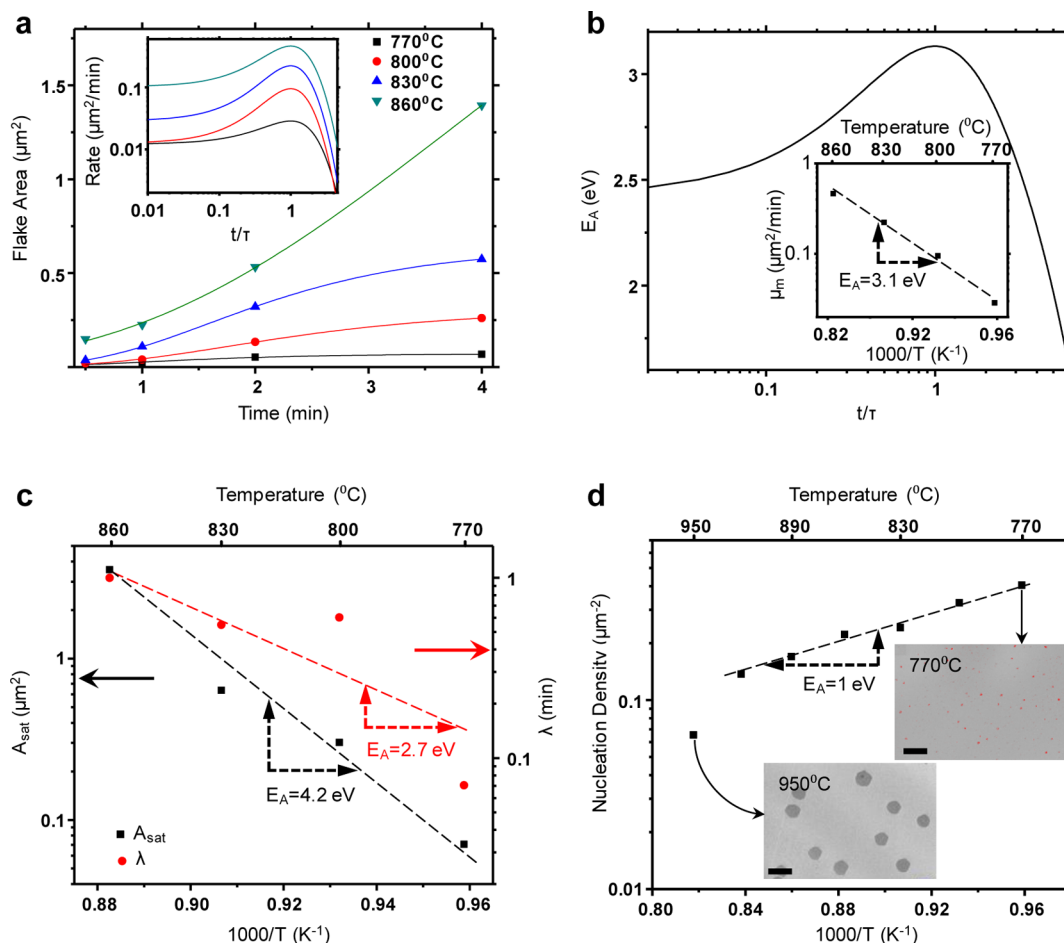
Figure 3. Quantitative kinetics. (a) Gompertz fits for varied growth temperature. Inset: Growth rate as a function of inflection-point-normalized time. (b) Time-dependent activation energy (E_A). Inset: Arrhenius plot of the inflection point growth rates. (c) Arrhenius plots of the saturation area (A_{sat}, ■) and time lag (λ, ●). (d) An Arrhenius plot of the nucleation density across an extended temperature range. An Arrhenius fit with $E_A = 1$ eV suggesting an attachment-limited regime for nucleation. Deviation occurs for growth temperature >920 °C. Insets: Typical SEM micrographs of graphene samples obtained at 770 and 950 °C (scale bar: 1 μm).

where the time-dependent exponential function in eq 2 is replaced by an area-dependent logarithmic function. The solution of the mechanistic expressions (eqs 2 and 3) gives eq 1, which agrees well with our measured growth data. According to eq 1, even for increased growth times, continuous surface covering cannot be obtained in some cases. However, if the hydrocarbon flow is increased, full covering could be achieved. Indeed, we could obtain continuous graphene films by increasing the ethylene partial pressure 3-fold or more.

Figure 2a shows an SEM micrograph of one such continuous monolayer showing small (<1 μm^2) hexagonal secondary flakes. Besides these secondary layers, spherical particles (<100 nm in diameter) are noted. Nanoauger spectroscopy suggested that these dots are copper oxide and chlorine agglomerates, most likely a product of oxidation upon exposure to ambient air and surface pretreatment by standardized HCl procedures during copper foil manufacturing (Figure S4). It remains for further investigation whether these particles cause pinhole formation on the as-grown graphene or act as nucleation centers. Secondary layer formation was confirmed by detailed Raman analysis (Figure 2b−d). Monolayer graphene accounts for over 98.4% of the measured area ($I_{G'}/I_G = 1.82 \pm 0.25$ (±1 S.D.)), with the remaining area mostly bilayer. Spatially resolved Raman spectroscopy over 150 μm^2 shows bilayer regions (blue) in addition to submicrometer juvenile bilayers (green) (Figure

2b). Interestingly, negligible defects were observed, even at the edges of these bilayer regions, with an I_D/I_G of 0.09 ± 0.02 (±1 S.D.). Measured electron mobilities of the order of 3600 cm^2 V^{-1} s^{-1} also support the low defect density observed here.

Thus far we have detailed one possible explanation of the fundamental mechanisms that govern the time-dependent kinetics of graphene growth. We now focus on quantifying the thermodynamic behavior of the graphene growth by extracting information pertaining to the activation energy pathways. Figure 3a shows the mean flake area as a function of growth time and the associated fittings at different temperatures.

To extract the activation energy, we first calculated the growth rates at each time point for different temperatures. Note that the inflection point shifts with increasing temperature, indicating that the time scales at each temperature are disparate. Using these time scales without normalization is unsuitable, as the activation energy is then a measure of particular growth reactions taking place at different times at each temperature. Thus, time has been rescaled to the characteristic time at the inflection point, thereby aligning the growth rates for each temperature according to equivalent reactions. The inset of Figure 3a confirms the initial increase in the growth rate attributed to the gradual increase of the graphene flake area that isolates the reactants from detrimental copper sublimation. The

postinflection decrease in growth rate is attributed to a reduction in the available copper surface necessary for hydrocarbon adsorption.

Activation energies were obtained as a function of dimensionless normalized time (Figure 3b). It is known that the time-dependent activation energy is associated with dispersive reaction kinetics.[33] The overall ensemble-averaged activation energy first increased from 2.4 eV to a maximum of 3.1 eV (Figure 3b) and then became vanishingly small when the growth saturates and stops. Here the flake area approached an asymptotic value representing the maximum attainable flake size at a certain supply rate of hydrocarbon. As a result of rapid precursor-to-reactant catalytic conversion, the saturation area (A_{sat}) showed an Arrhenius-type increase (E_A = 4.2 eV) with rising growth temperature (Figure 3c). This strong temperature dependence and the associated thermodynamics is the subject of future study.

Figure 3c also illustrates the time lag (λ) which provides a measure of the hindrance at very early stage growth which affects the growth initiation and growth rate. While the temperature increase certainly results in faster graphene growth, due to the thermal enhancement of the catalytic reactions, it also delays the time that is required for the growth to reach the maximum rate. In our case, copper sublimation is believed to extend the incubation period of the growth, as it can induce carbon reactant desorption and impede the growth until the flakes enlarge, which in turn would reduce the sublimation rate.[34] Thus, the effect of the sublimation manifests as an increased time lag (λ) at high temperature. The associated Arrhenius plot suggests a 2.7 eV barrier for this lagging effect, which is consistent with the initial activation energy of 2.4 eV. These activation energies agree well with the heat of sublimation of copper: 2.5 eV near 1000 °C.[35] To avoid the deleterious effects of copper sublimation at high temperatures, the total pressure of the CVD chamber can be raised to shift the equilibrium phase of the copper toward a solid regime, the results of which will be reported elsewhere.

The time-dependent behavior of the activation energy raises the question of which activation energy value should be used to accurately define the rate-limiting reaction. The initial growth rate is certainly slower than the growth at the inflection point. Since a reduced growth rate may indicate an increased energy barrier, the initial activation energy may be misinterpreted to be larger than the energy at the inflection point, which would contradict our experimental observations (2.4 eV vs 3.1 eV). However, this could only be the case when comparing two reactions directly. Rather, the lower initial activation energy indicates a reactant-population-limited growth at the beginning of flake enlargement. If we consider bacterial population growth studies[36] where Gompertzian kinetics is widely applied, it is the growth rates at the inflection points that are taken into account as they are independent of population dynamics occurring prior to inflection point.[37] Similarly, in determining the rate-limiting step in copper-catalyzed graphene CVD, it can be inferred that the activation energy assessed from the growth rates at the inflection points would represent the best density configuration of the cascade reactions that cause the dispersive kinetics.

To define the rate-limiting step using the activation energy at the inflection point (3.1 eV) we account for the successive processes of: (a) hydrocarbon adsorption on copper; (b) surface diffusion; (c) catalytic dissociation/dehydrogenation; and (d) graphene lattice construction. It is very unlikely that the process is limited by atomic carbon adsorption onto the dominant surface orientations on annealed copper foils as no significant pyrolysis of ethylene was noted by in situ mass spectrometry (Figure S1b). Moreover, the energy barrier of direct carbon adatom adsorption is extremely large (4.8−6.1 eV for Cu (111) and Cu(100)).[38] The energy barrier for hydrocarbon attachment on copper is an order of magnitude lower,[13] and as such it is far from our observed activation energies. Diffusion effects can be ruled out as the energy barrier for reactant diffusion on copper is <1.0 eV.[16,39] In the case of lattice attachment, the edge formation energy of graphene on copper was calculated to be 1.0 eV,[14] which is also significantly smaller than our measured 3.1 eV. Lastly, the catalytic dissociative dehydrogenation of ethylene on copper can pose higher energy barriers (>2 eV) close to our activation energy.[40−43] Therefore, we propose that the rate-limiting step is the dissociative dehydrogenation of ethylene on copper to produce the active carbon reactants that attach to the edge of the growing graphene lattice.

A different rate-limiting step, assuming it to be carbon adatom attachment, has been reported for methane-based graphene growth on copper, with an activation energy of 2.6 eV.[9] Here a monomolecular-like Avrami growth was observed. Such growth is incompatible with our data and model. The disparity between ethylene- and methane-based growths may stem from distinct reaction cascades for each precursor. Since methane does not undergo carbon−carbon dissociation, the associated dehydrogenation reactions results in different kinetic behaviors, which unlike our case may not be dispersive in time. However, uncertainty lies in the absence of sufficient growth data that resolves the very early stages of the methane-based graphene CVD. Such time resolution would require very small amounts of precursor input at gas dwell times much shorter than the measurement time scales. Otherwise, the data may only display the growth after the inflection point, even if the growth is sigmoidal, in which case it may not be possible to distinguish whether the growth kinetics is in fact Avrami or Gompertzian. Indeed, if we ignore the early stage, the Gompertz function is not dissimilar to the Avrami model.

To further elucidate the differences between methane and ethylene precursors for graphene growth on copper, we have measured the areal nucleation density as a function of temperature. Unlike the enlarged flakes that were not sparse above 860 °C, the nucleations were suitably sparse for discrete observation at even higher temperatures. Figure 3d shows the corresponding Arrhenius curve for the nucleation density (number of nucleation sites per unit area). A decrease in the nucleation density with respect to growth temperature is clearly seen, in agreement with previous reports.[3,9] To explain this behavior we first rule out the initial quality effect of copper surface, as in our case the annealing condition was consistent for all growths, ensuring invariant catalyst morphology and crystallinity of the copper surfaces prior to graphene nucleation. Unlike graphene lattice enlargement, the nucleation of graphene is controlled by defect sites that initiate crystallization from an initial supersaturated state of active carbon reactants. This supersaturation is depleted over a time scale much smaller than our data could resolve. If the limiting effect was the amount of the initial carbon reactants, an increase in the nucleation density would have been observed with increasing temperature. However, our experimental findings suggest otherwise. Indeed, the rate increase in the carbon capture is more dominant than the increase in the rate of new nucleations, as the surface diffusion rate may also increase with temperature.
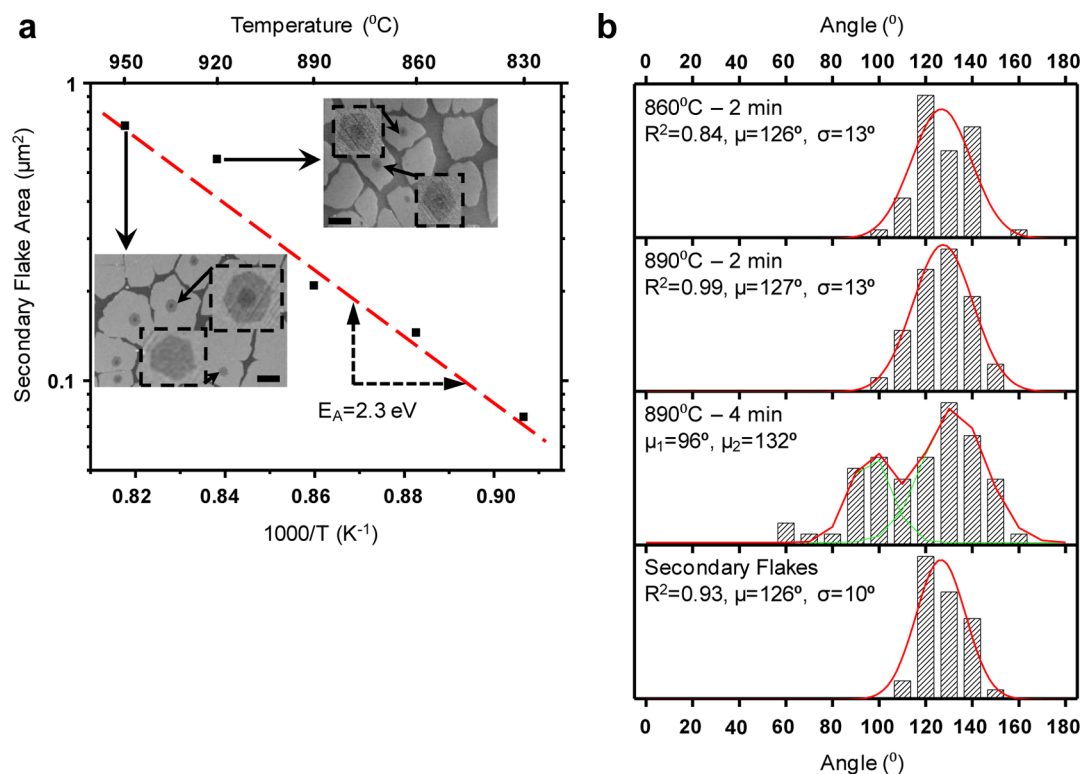
Figure 4. Flake morphology. (a) Arrhenius plot for secondary flake growth. Insets: Example SEM micrographs of secondary nucleations at 950 and 920 °C (scale bar: 1 μm). (b) Time evolving distribution of the edge angles of primary and secondary flakes. Narrow, single peak distributions at 120° indicate strong hexagonality. Increasing temperature from 860 to 890 °C results in improved hexagonality due to the onset of stable edge formation. Further increases in time from 2 to 4 min (890 °C) result in flake coalescence, which randomizes flake morphology by inducing substrate-dependent preferential growth directions. Secondary flakes show narrow Gaussian distribution (red/green curves) around 120° (σ = 10°), as they are less prone to detrimental copper sublimation effects.

Figure 3d suggests a nucleation activation energy of 1 eV, with an exception above ca. 920 °C, where the nucleation regime is believed to change from attachment-limited to desorption-limited, due to increased carbon removal from the copper surface. A similar activation energy and high temperature deviation have also been reported for methane-based graphene CVD on copper, albeit ca. 50 °C lower than our result.[9] This disparity in the deviation temperature can be attributed to the lower energy barrier for catalytic dehydrogenation of ethylene on copper compared to methane.[13]

While no further nucleations were observed for the main graphene layer after the near instantaneous nucleations, secondary layers of graphene emerge around the nucleation centers of the already growing graphene flakes (Figure 4a). These secondary nucleations were only observed under larger flakes, resulting in smaller flakes enlarging and adhering to the top layer from their underside.[44] The growth of these secondary layers continued until the first monolayer completely covered the surface. The top layer prohibited further carbon intake. Figure 4a illustrates the temperature dependence of the secondary flake sizes for a 4 min growth. There was no observable secondary nucleation present for shorter growth durations, especially at reduced growth temperatures. A more accurate study is ongoing. The apparent activation energy of this secondary layer growth was 2.3 eV, which is less than the activation energy of the primary layer. This result may be explained by the limited number of active reactants beneath the first flake. The first flake may capture all of the active reactants passing by, both from the front and back of the extending edge

in the continual influx of carbon precursor, whereas the secondary flake can only capture active reactants that have undergone the dissociative dehydrogenation cascades underneath the associated first flake without newly adsorbed precursor. Continued experimental and theoretical work is needed before a better understanding of such catalysis is obtained.

The effect of inhibited copper sublimation is evident from the shape of the secondary flakes. Though the associated flakes are smaller in area than the primary flakes (less than half the size), the morphologies are substantially more hexagonal with a mean (μ) vertex angle of 126° and a standard deviation (σ) of 10° (Figure 4b) compared to those of the primary flakes at the initial growth stages. This observation supports the postulate that reduced copper sublimation allows graphene to gain 6-fold symmetry independent of the copper's 4-fold symmetry.[27] In addition to the secondary flake morphology, Figure 4b also shows the evolution of the primary flake morphology. Smaller primary flakes (<0.5 μm in diameter) for a 2 min growth at 860 °C tended to be more circular (R^2 = 0.84, μ = 126°, σ = 13°) indicating a less stable morphology adopted prior to the formation of stable edge fronts. As the edges become increasingly stable (i.e., same growth time at higher temperature, 890 °C), the angle distribution forms a single Gaussian peak displaying a high degree of hexagonality (R^2 > 0.99, μ = 127°, σ = 13°) on those flakes that are large and far apart from one another (>half of the primary flake diameter). Following further growth (>2 min), these larger flake boundaries approach one another, coalesce, and induce preferential growth

directions toward the remaining unoccupied regions of the copper surface (Figure S5), which accounts for the angular shift (two distinct Gaussians evolve at 100° and 130°). In comparison with the low-pressure-CVD-based four-lobed graphene flakes,[27] hexagonality is generally more apparent in our CVD results as the total pressure was two or three orders of magnitude higher, thereby largely suppressing copper sublimation. This observation also confirms the detrimental effect of copper sublimation on the graphene flake morphology.

We have presented a sigmoidal growth model to account for the graphene CVD on copper. The time and temperature dependence of flake area and morphology suggests that the growth is driven by the continual hydrocarbon adsorption on the copper surface, rather than crystallization from an initial supersaturated surface pool of carbon adatoms. Copper sublimation plays an important role in inhibiting growth reactions, enhancing surface carbon desorption, thereby initially hindering growth after nucleation. When carbon reactants on the surface diffuse beneath the enlarging graphene flakes, they are prevented from desorbing and are isolated from detrimental copper sublimation. At first, this protection instigates a growth rate increase as the graphene flakes enlarge, but as the adsorption-available bare copper surface reduces in size, the growth similarly reduces, saturating the flake area. Only if the continual hydrocarbon input to the system is large can a full covering be obtained. The proportionality of the growth rate with an available amount of active carbon reactants and dispersive kinetic processes for converting simple hydrocarbon adsorbates to the active carbon reactants can be modeled by a Gompertz differential model, with a strongly time-dependent activation energy. From the maximum activation energy of 3.1 eV we propose the catalytic dissociative dehydrogenation to be the rate-limiting step for graphene CVD on copper. In conjunction with a Gompertzian growth, our analysis provides new evidence of the complex catalysis underlying graphene chemical deposition that has not been hitherto proposed.

■ ASSOCIATED CONTENT

ⓢ Supporting Information

Methods section and additional data from mass spectroscopy, electron microscopy, and nano Auger spectroscopy. This material is available free of charge via the Internet at http://pubs.acs.org.

■ AUTHOR INFORMATION

Corresponding Author
*E-mail: parkh@ethz.ch.

Notes
The authors declare no competing financial interest.

■ ACKNOWLEDGMENTS

■ REFERENCES

(1) Li, X.; Cai, W.; An, J.; Kim, S.; Nah, J.; Yang, D.; Piner, R.; Velamakanni, A.; Jung, I.; Tutuc, E.; Banerjee, S. K.; Colombo, L.; Ruoff, R. S. *Science* **2009**, *324* (5932), 1312−1314.

(2) Kim, K. S.; Zhao, Y.; Jang, H.; Lee, S. Y.; Kim, J. M.; Kim, K. S.; Ahn, J.-H.; Kim, P.; Choi, J.-Y.; Hong, B. H. *Nature* **2009**, *457* (7230), 706−710.

(3) Li, X.; Magnuson, C. W.; Venugopal, A.; An, J.; Suk, J. W.; Han, B.; Borysiak, M.; Cai, W.; Velamakanni, A.; Zhu, Y.; Fu, L.; Vogel, E. M.; Voelkl, E.; Colombo, L.; Ruoff, R. S. *Nano Lett.* **2010**, *10* (11), 4328−4334.

(4) Ni, G.-X.; Zheng, Y.; Bae, S.; Kim, H. R.; Pachoud, A.; Kim, Y. S.; Tan, C.-L.; Im, D.; Ahn, J.-H.; Hong, B. H.; Özyilmaz, B. *ACS Nano* **2012**, *6* (2), 1158−1164.

(5) Tsen, A. W.; Brown, L.; Levendorf, M. P.; Ghahari, F.; Huang, P. Y.; Havener, R. W.; Ruiz-Vargas, C. S.; Muller, D. A.; Kim, P.; Park, J. *Science* **2012**, *336* (6085), 1143−1146.

(6) Coraux, J.; N'Diaye, A. T.; Engler, M.; Busse, C.; Wall, D.; Buckanie, N.; zu Heringdorf, F.-J. M.; van Gaste, R.; Poelsema, B.; Michely, T. *New J. Phys.* **2009**, *11*, 023006.

(7) Loginova, E.; Bartelt, N. C.; Feibelman, P. J.; McCarty, K. F. *New J. Phys.* **2008**, *10* (9), 093026.

(8) McCarty, K. F.; Feibelman, P. J.; Loginova, E.; Bartelt, N. C. *Carbon* **2009**, *47* (7), 1806−1813.

(9) Kim, H.; Mattevi, C.; Calvo, M. R.; Oberg, J. C.; Artiglia, L.; Agnoli, S.; Hirjibehedin, C. F.; Chhowalla, M.; Saiz, E. *ACS Nano* **2012**, *6* (4), 3614−3623.

(10) Liu, L.; Zhou, H.; Cheng, R.; Chen, Y.; Lin, Y.-C.; Qu, Y.; Bai, J.; Ivanov, I. A.; Liu, G.; Huang, Y.; Duan, X. *J. Mater. Chem.* **2012**, *22* (4), 1498−1503.

(11) Li, X.; Cai, W.; Colombo, L.; Ruoff, R. *Nano Lett.* **2009**, *9* (2), 4268−4272.

(12) Bhaviripudi, S.; Jia, X.; Dresselhaus, M. S.; Kong, J. *Nano Lett.* **2010**, *10* (10), 4128−4133.

(13) Zhang, W.; Wu, P.; Li, Z.; Yang, J. *J. Phys. Chem. C* **2011**, *115* (36), 17782−17787.

(14) Luo, Z.; Kim, S.; Kawamoto, N.; Rappe, A. M.; Johnson, A. T. C. *ACS Nano* **2011**, *5* (11), 9154−9160.

(15) Riikonen, S.; Krasheninnikov, A. V.; Halonen, L.; Nieminen, R. M. *J. Phys. Chem. C* **2012**, *116* (9), 5802−5809.

(16) Hayashi, K.; Sato, S.; Ikeda, M.; Kaneta, C.; Yokoyama, N. *J. Am. Chem. Soc.* **2012**, *134* (30), 12492−12498.

(17) Treier, M.; Pignedoli, C. A.; Laino, T.; Rieger, R.; Müllen, K.; Passerone, D.; Fasel, R. *Nat. Chem.* **2011**, *3* (1), 61−67.

(18) Avrami, M. *J. Chem. Phys.* **1939**, *7* (12), 1103−1112.

(19) Winsor, C. P. *Proc. Natl. Acad. Sci. U.S.A.* **1932**, *18* (1), 1−8.

(20) Lin, M.; Ying Tan, J. P.; Boothroyd, C.; Loh, K. P.; Tok, E. S.; Foo, Y.-L. *Nano Lett.* **2006**, *6* (3), 449−452.

(21) Chaleepa, K.; Szepes, A.; Ulrich, J. *Chem. Phys. Lipids* **2010**, *163* (4−5), 390−396.

(22) Foubert, I.; Dewettinck, K.; Vanrolleghem, P. A. *Trends Food Sci. Technol.* **2003**, *14* (3), 79−92.

(23) Kloek, W.; Walstra, P.; van Vliet, T. *J. Am. Oil Chem. Soc.* **2000**, *77* (4), 389−398.

(24) Vanhoutte, B.; Dewettinck, K.; Foubert, I.; Vanlerberghe, B.; Huyghebaert, A. *Eur. J. Lipid Sci. Technol.* **2002**, *104* (8), 490−495.

(25) Zwietering, M.; Jongenburger, I.; Rombouts, F.; Van't Riet, K. *Appl. Environ. Microbiol.* **1990**, *56* (6), 1875−1881.

(26) Nie, S.; Wu, W.; Xing, S.; Yu, Q.; Pei, S.; McCarty, K. F. *Arxiv preprint arXiv:1202.1031*, **2012**.

(27) Wofford, J. M.; Nie, S.; McCarty, K. F.; Bartelt, N. C.; Dubon, O. D. *Nano Lett.* **2010**, *10* (12), 4890−4896.

(28) Egloff, G. *The reactions of pure hydrocarbons*; Reinhold Publishing Corporation: New York, 1937.

(29) Yazyev, O. V.; Pasquarello, A. *Phys. Rev. Lett.* **2008**, *100* (15), 156102.

(30) Lizzit, S.; Baraldi, A. *Catal. Today* **2010**, *154* (1−2), 68−74.

(31) Plonka, A. *Annu. Rep. Prog. Chem. Sect. C: Phys. Chem.* **2001**, *97*, 91−147.

(32) Siebrand, W.; Wildman, T. A. *Acc. Chem. Res.* **1986**, *19* (8), 238−243.

(33) Skrdla, P. J. *Langmuir* **2012**, *28* (10), 4842−4857.

(34) Zhan, L.; Qiu, Z.; Xu, Z. *Sep. Purif. Technol.* **2009**, *68* (3), 397−402.

(35) Simon, N.; Drexler, E.; Reed, R. P. *Properties of copper and copper alloys at cryogenic temperatures*; US National Institute of Standards and Technology: Gaithersburg, MD, 1992.

(36) Cayré, M. a. E.; Vignolo, G.; Garro, O. *Food Microbiol.* **2003**, *20* (5), 561−566.

(37) Zwietering, M.; De Koos, J.; Hasenack, B.; De Witt, J.; Van't Riet, K. *Appl. Environ. Microbiol.* **1991**, *57* (4), 1094−1101.

(38) Zhao, L.; Rim, K. T.; Zhou, H.; He, R.; Heinz, T. F.; Pinczuk, A.; Flynn, G. W.; Pasupathy, A. N. *Solid State Commun.* **2011**, *151* (7), 509−513.

(39) Wu, P.; Zhang, W.; Li, Z.; Yang, J.; Hou, J. G. *J. Chem. Phys.* **2010**, *133* (7), 071101−4.

(40) Sinfelt, J. H.; Carter, J. L.; Yates, D. J. C. *J. Catal.* **1972**, *24* (2), 283−296.

(41) Franklin, J. L.; Field, F. H. *J. Chem. Phys.* **1953**, *21* (11), 2082−2083.

(42) Sinfelt, J. H.; Yates, D. J. C. *J. Catal.* **1967**, *8* (1), 82−90.

(43) Chen, Y.; Vlachos, D. G. *J. Phys. Chem. C* **2010**, *114* (11), 4973−4982.

(44) Fan, L.; Li, Z.; Xu, Z.; Wang, K.; Wei, J.; Li, X.; Zou, J.; Wu, D.; Zhu, H. *AIP Adv.* **2011**, *1*, 032145.